

UC Irvine

UC Irvine Previously Published Works

Title

Rapid Intramitochondrial Zn²⁺ Accumulation in CA1 Hippocampal Pyramidal Neurons After Transient Global Ischemia: A Possible Contributor to Mitochondrial Disruption and Cell Death.

Permalink

<https://escholarship.org/uc/item/8x75m5cn>

Journal

Journal of neuropathology and experimental neurology, 78(7)

ISSN

0022-3069

Authors

Yin, Hong Z
Wang, Hwai-Lee
Ji, Sung G
et al.

Publication Date

2019-07-01

DOI

10.1093/jnen/nlz042

Peer reviewed

Rapid intra-mitochondrial Zn²⁺ accumulation in CA1 hippocampal pyramidal neurons after transient global ischemia: A possible contributor to mitochondrial disruption and cell death

Short title: Mitochondrial Zn²⁺ accumulation after TGI

Hong Z. Yin, MD ¹, Hwai-Lee Wang ^{1,3}, Sung G. Ji ², Yuliya V. Medvedeva, PhD ¹, Guilian Tian, PhD ¹, Afsheen Bazrafkan ¹, Niki Maki ¹, Yama Akbari, MD, PhD ¹, and John H. Weiss, MD, PhD ^{1,2}

From the ¹Department of Neurology , and the ²Department of Anatomy & Neurobiology, University of California, Irvine and the ³Graduate Institute of Clinical Medical Science, China Medical University, Taichung, Taiwan

Address correspondence to:

John H. Weiss, MD, Ph.D.
2101 Gillespie Building
Department of Neurology, University of California, Irvine
Irvine, CA 92697-4292
Tel: (949) 824-6774
Fax: (949) 824-1668
E-mail: jweiss@uci.edu

Author contributions and conflicts

All authors contributed to the execution of experiments, data analysis, and/or writing and editing of the manuscript. All have read and approve of the manuscript as submitted.

H.Y. No conflict
H.W. No conflict
S.J. No conflict
Y.M. No conflict
G.T. No conflict
A.B. No conflict
N.M. No conflict
Y.A. No conflict
J.W. No conflict

Supported by NIH grants NS096987 and NS100494 (JHW), and the American Heart Association grants 17GRNT33410181 (JHW) and 16PRE29560003 (SGJ).

Abstract

Despite the huge costs of ischemic neuronal injury, neuroprotective interventions in humans remain elusive, in part reflecting incomplete knowledge of the critical early events. Emerging evidence implicates Zn^{2+} as an important early contributor. CA1 pyramidal neurons undergo selective delayed degeneration after transient global ischemia (TGI), and Zn^{2+} has been implicated in the injury. *In vitro* studies have indicated that Zn^{2+} enters mitochondria and has potent effects on their function. In addition, Zn^{2+} accumulates in CA1 mitochondria after ischemia in hippocampal slice and whole animal models, and appears to contribute to their dysfunction. However, the relationship between mitochondrial Zn^{2+} accumulation and their disruption has not been examined at the ultrastructural level *in vivo*, reflecting the difficulty in assessing dynamics of labile (loosely bound) Zn^{2+} . We employ a cardiac arrest model of ischemia, combined with Timm's sulfide silver labeling, which inserts electron dense metallic silver granules at sites of labile Zn^{2+} accumulation, and use transmission electron microscopy (TEM) to examine subcellular loci of the Zn^{2+} accumulation. In line with prior studies, TGI induced damage to CA1 was far greater than to CA3 pyramidal neurons, and was substantially progressive in the hours after reperfusion (being significantly greater after 4 than 1 h recovery). Intriguingly, TEM examination of Timm stained sections revealed substantial Zn^{2+} accumulation in many post-ischemic CA1 mitochondria, which was strongly correlated with their swelling and disruption. Furthermore, paralleling the evolution of neuronal injury, both the number of mitochondria containing Zn^{2+} and the degree of their disruption were far greater at 4 than 1 h recovery. These data provide the first direct characterization of Zn^{2+} accumulation in CA1 mitochondria after *in vivo* TGI, and further support the idea that mitochondria constitute an early and potentially targetable locus of Zn^{2+} effects in ischemia that contributes to mitochondrial damage and neuronal injury.

Keywords: zinc; excitotoxicity; mitochondria; ischemia; rat; stroke; hippocampus

Abbreviations: cardiac arrest (CA); cardiopulmonary resuscitation (CPR); hippocampal pyramidal neuron (**HPN**); metallothionein (MT); mitochondrial Ca^{2+} uniporter (MCU); N-methyl-D-aspartate (NMDA); outer membrane (OM); oxygen glucose deprivation (OGD); paraformaldehyde (PFA); phosphate buffered saline (PBS); Toluidine blue (TB); transient global ischemia (TGI); transmission electron microscopy (TEM); vanadium acid fuchsin (VAF).

Introduction

Brain ischemia is a leading cause of death and disability worldwide, but there are as yet no effective neuroprotective therapies. Many studies implicate “excitotoxicity” caused by excessive glutamate release as an important contributor and have largely focused on consequences of rapid Ca^{2+} entry through NMDA receptors. However, NMDA targeted therapies have shown limited clinical efficacy [1, 2]. Further studies have implicated contributions of another divalent cation, Zn^{2+} [3-7]. Despite high total levels of brain Zn^{2+} (100-200 μM), almost all of it is bound or sequestered, and free cytosolic levels are generally subnanomolar. However, a small portion (~10%) of brain Zn^{2+} is loosely bound (termed labile Zn^{2+}); this pool largely comprises Zn^{2+} present in certain pre-synaptic vesicles (most conspicuously in the mossy fiber pathway) [8], from which it can be co-released with glutamate upon synaptic activation [9-11], and can be visualized using a histochemical technique (Timm’s sulfide silver labeling), or with membrane permeant fluorescent indicators [8, 12, 13]. Indeed, indicating its specificity, Timm’s labeling is completely absent in brains of knockout mice lacking the vesicular Zn^{2+} transporter, ZnT3 [14]. In pathological conditions of ischemia or prolonged seizures, associated with strong synaptic activation, there is release of this presynaptic Zn^{2+} , along with appearance of new labile Zn^{2+} in somata of some hippocampal pyramidal neurons (and other forebrain neurons)[3-5, 11], reflecting a combination of synaptically released Zn^{2+} that can enter postsynaptic neurons through various routes (“ Zn^{2+} translocation”), and Zn^{2+} mobilization from buffers (particularly metallothionein-III; **MT-III**) already present in the postsynaptic neurons, in response to oxidative

stress and acidosis [15, 16].

However, the redistribution of labile Zn^{2+} has never been examined at the ultrastructural level. Multiple studies have indicated that Zn^{2+} can induce potent effects on mitochondria *in vitro* and after transient ischemia *in vivo* [6, 16-19]. In addition, we have carried out studies using hippocampal slices subjected to prolonged oxygen glucose deprivation (**OGD**) to model acute ischemia, and found that early cytosolic Zn^{2+} rises and mitochondrial Zn^{2+} entry appears to contribute to the acute hippocampal pyramidal neuron (**HPN**) injury [20, 21]. Furthermore, after shorter (sublethal) episodes of OGD, there was a gradual recovery of the early cytosolic Zn^{2+} elevations accompanied by progressive and persistent Zn^{2+} accumulation in mitochondria of CA1 (but not CA3) neurons, that appeared to contribute to delayed mitochondrial swelling [22], possibly consistent with the selective delayed degeneration of these neurons after transient ischemia [23-25]. However, whereas these *in vitro* observations support the possibility that mitochondria are critical loci of early Zn^{2+} effects *in vivo*, this question has not as yet been directly examined in animals.

In the present study, we employ a rat asphyxial cardiac arrest (**CA**) model of transient global ischemia (**TGI**), which provides the advantage over focal ischemia that the entire brain is subjected to the same duration of ischemia, such that regional differences in outcome largely reflect differences in susceptibility. Using this model system, we aimed, for the first time, to examine the redistribution of Zn^{2+} into mitochondria and its potential contribution to mitochondrial disruption and neuronal injury. Such a study requires an ultrastructural assessment, to correlate Zn^{2+} accumulation with morphology of individual mitochondria, and the presently employed technique of Timm's labeling (which inserts electron dense silver deposits *in situ* at subcellular sites of labile Zn^{2+} accumulation) combined with transmission electron microscopy (**TEM**) would seem ideally suited for such an investigation. Present findings, which show for the first time progressive Zn^{2+} accumulation in CA1 mitochondria after *in vivo* TGI to be strongly correlated with their physical disruption, provide new support for a direct contributory role of the mitochondrial Zn^{2+} in the delayed and progressive mitochondrial damage and cell death of these neurons.

Materials and Methods

Ethics statement

This study was carried out in accordance with the recommendations from the Guide for the Care and Use of Laboratory Animals of the National Institutes of Health and approved by the Institutional Animal Care and Use Committee of the University of California, Irvine.

Animals

Experiments were performed using male Wistar rats (Charles River Laboratories, Wilmington, MA) weighing 300-350 g (approximately 8-12 weeks). After applying the inclusion criterion that chest compressions lasted shorter than 1min (as previously described) [26], the final number of rats included for data analysis was 25. Upon arrival, rats were maintained in a 12-h light/12-h dark (6:00 am/6:00 pm) cycle and fed standard rat chow. They are handled for at least five days for acclimation to the researchers and their new environment.

Cardiac arrest and resuscitation

This study utilizes an asphyxial CA model largely as previously described [26, 27]. Rats were calorically restricted to 25% of normal food intake 14 h prior to CA experiment. Rats were intubated using a 14-gauge endotracheal tube (B. Braun Melsungen AG, Melsungen, Germany), connected to a TOPO mechanical ventilator (Kent Scientific, Torrington, CT) and isoflurane vaporizer for delivery of 2% isoflurane and 50% O₂ and 50% N₂ gas during surgical preparation for CA. Femoral artery and vein cannula allowed for monitoring of blood pressure and heart rate, and administration of intravenous medication. Invasive arterial blood pressure was measured continuously using a transducer (CWE Inc., Ardmore, PA).

CA experiments began at “minute 0”, when the isoflurane level was reduced to 1-1.5% to prepare for anesthesia wash out and inhaled gas was switched to 100% O₂. After two minutes, isoflurane was stopped to wash out anesthesia, neuromuscular blockade initiated with 1mL of intravenous Vecuronium (2mg/kg) injected with 1mL of heparinized saline, and the inlet was

disconnected from oxygen to allow room air to be mechanically delivered to the rat. At minute 5, asphyxial CA was induced by turning the ventilator off and clamping the ventilator tubing. CA time was defined as systolic blood pressure less than 30 and pulse pressure of 10 or less. Baseline arterial blood gas (**ABG**) measurements (Abaxis, Union City, CA) were obtained within 30 min prior to initiation of asphyxia. Durations of asphyxia were all between 8 and 9 minutes. In the last minute of asphyxia, as the ventilator is being reconnected and turned on, 0.4 ml epinephrine (0.01mg/kg) and 0.5 ml bicarbonate (1.0 mmol/kg) are given to stimulate the sympathetic nervous system and manage acidosis, respectively. Of 17 rats subjected to asphyxial CA used in the data analysis, the mean duration of asphyxia was 8.5 ± 0.1 min, yielding CA durations of 6.8 ± 0.2 min (mean \pm SEM). Cardiopulmonary resuscitation (CPR, manual sternal compressions at 180-240 per minute) was performed and continued until return of spontaneous circulation (**ROSC**). ABGs were obtained 10-min post-ROSC, to assess ventilation and modify ventilator settings as necessary. Over the next 1 hr post ROSC vessels were decannulated and rats were extubated.

VAF / toluidine blue staining and confocal imaging of mitochondrial morphology

One or 4 h after CPR, animals were anesthetized with isoflurane, and perfused transcardially with phosphate buffered saline (**PBS**) for 2 min, followed by 4% paraformaldehyde (**PFA**) in PBS for 10 min. The brains were post-fixed in 4% PFA /1% gluteraldehyde for 72 h, then PFA was exchanged for 30% sucrose (in PBS) for another 2 days, 30 μ m brain sections containing hippocampus were cut using a cryostat (ThermoFisher Scientific).

To assess neuronal injury, sections were stained with vanadium acid fuchsin (**VAF**)/toluidine blue (toluidine blue (**TB**) largely as described [28]. In brief, slices were stained with VAF for 1-2 min, washed with PBS, incubated in 0.01% borax solution for 20-30 second, and rinsed in distilled water. Finally, brain slices were cleared by acetate buffer (PH 3.3) for 30 seconds and counterstained with 0.025% toluidine blue for 20-30 seconds. Stained slices were assessed using light microscopy.

To assess mitochondrial morphology, sections were labeled with primary antibodies against the mitochondrial outer membrane protein, translocase outer membrane-20 (**TOM20**; 1:200; Santa Cruz Biotechnology) and secondary anti-rabbit fluorescent antibodies (1:200, DyLight 488; Jackson ImmunoResearch). The sections were imaged using an inverted stage Nikon Eclipse Ti chassis microscope with a Yokogawa CSUX spinning disk head and a 100× (1.49 numerical aperture) objective and images acquired using a Hamamatsu electromultiplying CCD camera. Excitation (488 nm) was via a Coherent sapphire laser source synchronized with the camera, emission was monitored with a 525 (50) nm filter, and images were acquired using MicroManager ImageAcquisition software (version 1.4.16).

Cardiac perfusion and tissue sections preparation for Timm's labeling

In initial studies, brain sections were prepared in 2 ways (as outlined in Results). Our first attempts sought to maximize rapid Zn^{2+} fixation in situ; animals were perfused with 0.2% Na_2S in Millonig's buffer for 5 min to precipitate Zn^{2+} , followed by 4% PFA / 1% glutaraldehyde solution in PBS for the next 12 min. After perfusion the brains were removed and post-fixed using 2% PFA / 2% glutaraldehyde / 0.2% Na_2S , 4°C for 72 h, then placed into 30% sucrose solution in PBS for 48-72 h, followed by OCT embedding and cryostat sectioning (to 50 or 80 μm thickness).

Subsequent studies sought to optimize tissue preservation – to that aim rats were perfused transcardially with 4% PFA / 1% glutaraldehyde solution in PBS for 5 min, followed by 0.4% Na_2S / Millonig's buffer (0.12M; 0.002% CaCl_2 , 1.6% NaH_2PO_4 and 0.4% NaOH ; PH 7.3) for next 7 min to precipitate Zn^{2+} [29]. Brains were removed and post-fixed using 2% PFA / 2% glutaraldehyde / 0.2% Na_2S , 4°C overnight, prior to vibratome sectioning (again to 50 or 80 μm thickness).

For Timm's staining, slices were incubated in the dark in a solution containing 1 part solution A (1M AgNO_3), 20 parts solution B (2% hydroquinone and 5% citric acid in water), and 100 parts of solution C (30% gum arabic in water). Development was performed in the dark, was monitored by periodic evaluations under low light, and was terminated by washing in water. 80 μm slices were placed into PBS and processed for electron microscopy; 50 μm slices were analyzed under light microscopy.

Electron microscopy

For TEM analysis, we utilized ultrathin sections ($\sim 1\ \mu\text{m}$ thickness) from vibrotome or cryostat cut fixed brain slices, prepared largely as previously described [30] with small modifications. The sections were rinsed in PBS and post-fixed with 1% osmium tetroxide in PBS for 1 hour, then dehydrated in increasing serial dilutions of ethanol (70%, 85%, 95%, 100%), put into intermediate solvent propylene oxide (2 times for 10 min), and incubated in 1:1 mixture of propylene oxide/Spurr's resin for 1 h. Finally slices were embedded in Spurr's resin overnight. Ultrathin sections ($\sim 70\text{nm}$ thickness) were cut using a Leica Ultracut UCT ultramicrotome (Leica, Vienna, Austria) mounted on 150 mesh copper grids, stained with lead citrate and viewed using a JEOL 1400 electron microscope (JEOL, Tokyo, Japan). Images were captured using a Gatan digital camera (Gatan, Pleasanton, CA, USA).

Statistics and data analysis

All counts / ratings were carried out entirely by raters blinded to the experimental conditions (TEM, TOM-20), or verified via extensive sampling by blinded raters (VAF/TB).

For assessment of neuronal injury (VAF/TB) photomicrographs (40 x magnification) were obtained from each section. The rater examined the micrographs, and judged each identifiable neuron in the section as healthy or injured based upon criteria as described. For mitochondrial ratings of TEM images of sections from CA1, all evident mitochondria in images from CA1 pyramidal neurons were rated as to the presence of Timm's stain deposits (representing Zn^{2+}) and the integrity of the mitochondria, according to criteria as described. For measurement of TOM-20 labeled mitochondria, large neurons in the pyramidal cell layer were imaged using confocal microscopy. To control for differing behavior of mitochondria between cellular compartments, we focused our studies on mitochondria in the perinuclear region, in the plane of sharp focus. Images were imported into ImageJ software, and were adjusted to provide optimal discrimination of the apparent mitochondrial edges from background. Length and width

measurements were obtained on all clearly demarcated mitochondria adjacent to and surrounding the nuclear circumference.

To assess significance, either two-tailed t-test or one-way ANOVA with Tukey post-hoc analysis (indicated in each figure legend) was used, depending on the number of groups of comparison. All values are displayed as mean \pm standard error of the mean (SEM). All experiments were repeated at least 3 times.

Results

HPN injury after transient global ischemia (TGI)

Rats were subjected to asphyxial cardiac arrest (CA) as described (see **Materials and Methods**). After resuscitation followed by 1 h or 4 h of recovery, rats were perfused, and their hippocampi processed for histological analysis.

To assess overall injury to CA1 and CA3 pyramidal neurons, sections were stained with a modified acid fuchsin labeling procedure to identify acidophilic neurons (termed *vanadium acid fuchsin*, VAF labeling) [28], and counter stained with toluidine blue (TB; to assess morphology). Sections were examined and each identifiable neuron rated as healthy or injured. Healthy neurons showed distinct round nuclei surrounded by TB stained cytoplasm. Injured neurons were of two types; one subset that showed clear atrophy along with VAF (acidophilic) labeling in the cytoplasm indicative of early injury, whereas others showed severe swelling with loss of clear distinction between nucleus and surrounding cytoplasm, vacuolar changes, and absence of clear VAF labeling (**Fig. 1A, Left**). We noted that in comparison to control, episodes of global ischemia caused distinct and substantial injury to CA1 pyramidal neurons, with relatively little injury in CA3. In addition, the CA1 injury was greater after 4 h than after 1 h recovery, indicating apparent progression of the injury in the hours after the ischemic episode (**Fig. 1A, Right**).

To begin to address our questions concerning possible Zn^{2+} contributions to the injury, some sections were stained with a modified Timm's procedure (see **Materials and Methods**) to assess the presence and localization of labile Zn^{2+} , and examined under conventional brightfield microscopy (**Fig. 1B**). As discussed above, the Timm's technique detects labile or loosely bound

Zn²⁺ in tissues by using sulfide ion to precipitate the Zn²⁺ and “developing” the label (much as with photographic prints) via reduction and deposition of metallic silver at loci of the ZnS precipitates, and in brain appears to be entirely selective for Zn²⁺ [8, 14]. Note that in control slices, distinct Timm’s labeling, indicative of labile Zn²⁺, is most prominent in the mossy fiber boutons in the dentate gyrus, the hilus and extending along the CA3 pyramidal cell layer, but that labeling is largely absent in neuronal somata. Further note the substantial loss of Timm’s label from the mossy fibers 1 h after ischemia, with partial recovery of labeling after 4 h. Finally, note the appearance of weak Timm’s label in somata of CA1 neurons after ischemia that is greater with 4 than with 1 h recovery, indicative of some relocalization of labile Zn²⁺, paralleling the observed neuronal injury.

Figure 1. Global ischemia induces progressive neuronal injury and Zn²⁺ accumulation in CA1 pyramidal neurons. Rats were subjected to TGI followed by resuscitation as described. After 1 or 4 h recovery, rats were euthanized, perfused, and brain tissue removed for histological examination as described. Injury was assessed on hippocampal slices subjected to a modified acid fuchsin labeling procedure (VAF; detailed in Methods) and counter stained with toluidine blue; Zn²⁺ accumulation was assessed via Timm’s labeling (see **Materials and Methods**).

A. Global ischemia induced injury to hippocampal CA1 pyramidal neurons.
Left: Representative images. Hippocampal slices were photographed at low magnification (Bar = 500 μm), and CA1 and CA3 regions (indicated by blue and red rectangles, respectively) examined at higher magnification (Bar = 50 μm). While most neurons appear intact in control slices, note the increased numbers of VAF stained neurons as well as of severely swollen neurons (with vacuolar changes and loss of distinct nuclear outlines) after ischemia. Further note that these changes are more prevalent in CA1 than in CA3, and appear to increase from 1 to 4 h after ischemia (particularly in CA1). Examples of intact (arrow) and damaged (VAF +, triangle; swelling and vacuolar changes, circled) neurons are marked.

Right: Quantitative assessment. All discernable neurons were rated as intact or injured, and the percentages of CA1 and CA3 neurons determined to be injured within each hippocampal section were calculated. Note that the extent of neuronal injury was far greater in CA1 than in CA3, and that in CA1, it was significantly greater after 4 h than 1 h recovery. Bars represent mean ± SEM from 4 – 7 independent animals (comprising ≥ 1000 cells from CA1; ≥ 500 from CA3; with ≥ 3 sections counted for each animal; ** indicates p < 0.01 by one way ANOVA with Tukey post hoc).

B. Transient loss of mossy fiber Zn²⁺ and progressive Zn²⁺ accumulation in CA1 pyramidal neurons after transient global ischemia. Photomicrographs show low magnification images of Timm’s labeled hippocampal sections (Bar = 500 μm), and greater magnification images of the CA1 regions from the same sections (indicated by rectangles; Bar = 50 μm). Note the robust stain in the mossy fibers (indicative of presynaptic vesicular Zn²⁺) in control, and the substantial loss of this Zn²⁺ at 1 h recovery. Further note the appearance of some Zn²⁺ in the somata of CA1 pyramidal neurons that progresses from 1 h to 4 h after ischemia (a small amount of accumulation was also noted in some CA3 pyramidal neurons, not shown; Images are representative of ≥ 3 repetitions each condition).

Transient global ischemia induces mitochondrial swelling

Previous studies have suggested that mitochondria are likely to be important targets of Zn²⁺-

induced neuronal injury [19]. In light of our recent observations of protracted Zn^{2+} accumulation in CA1 mitochondria after OGD in hippocampal slice [22], we next sought to examine mitochondrial morphology in CA1 neurons after TGI. Sections were immunostained for the mitochondrial outer membrane marker, TOM-20, examined under confocal microscopy (1000x), and images obtained in the CA1 and CA3 pyramidal layers, largely as previously described [22]. For quantitative assessment, images were adjusted (using Image J software) to optimally discriminate mitochondrial borders from background, and perinuclear regions cropped from images and coded for blinded measurement of mitochondrial lengths and widths (see Materials and Methods). We found that OGD caused a marked “rounding-up” of the mitochondria with substantial decreases in their mean lengths, increases in their widths, and decreased length / width (L/W) ratios. Notably, whereas direct visual examination of the microscope fields yielded an impression that mitochondrial swelling and disruption were worse in CA1 than in CA3, and were greater after 4 than 1 h recovery, the quantification procedure did not confirm these differences (showing substantially decreased L/W ratios in all ischemic conditions) (**Fig. 2**). This was felt to reflect a limitation of the approach – as only mitochondria with distinct visualization of edges were amenable to measurement – and extreme swelling and consequent blurring of the borders of the most effected mitochondria precluded accurate assessment of levels of swelling towards the extreme end of the scale.

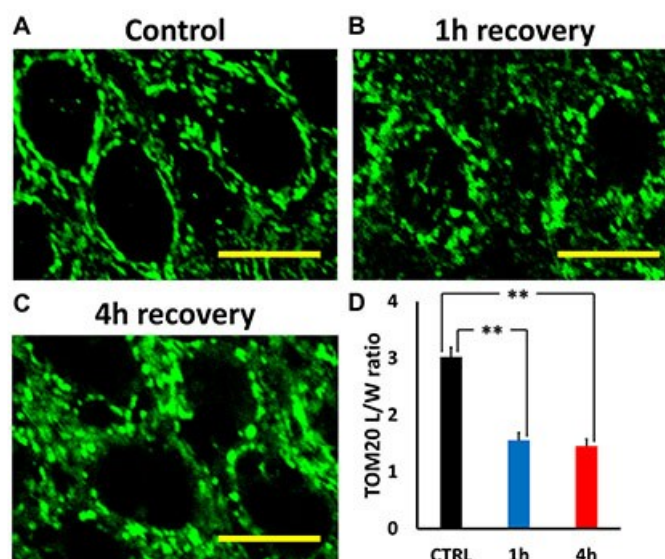


Figure 2. Ischemia disrupts mitochondrial morphology in CA1 pyramidal neurons.

Rats were subjected to TGI followed by 1 or 4h recovery. Hippocampal slices were immunostained using antibody against the mitochondrial outer membrane marker, TOM20, and examined under confocal microscopy (1000x).

A-C: Representative images of TOM20-labeled CA1 mitochondria. Note the generally elongated mitochondria seen in perinuclear regions of control (**A**), in contrast to the abundant fragmented and swollen mitochondria 1 or 4 h after ischemia (**B** and **C**; Bar = 10 μ m).

D: Ischemia impacts mitochondrial morphology. Lengths and widths of individual mitochondria were measured blindly (using ImageJ software) and length/width (L/W) ratios calculated to quantify morphological change (lower L/W ratios indicates rounding of mitochondria). The L/W ratio for all mitochondria measured in neurons from a single animal were averaged to produce a single, mean L/W ratio for that animal. Note the significant decrease in L/W ratio after ischemia. Bars represent mean L/W ratio \pm SEM from 4 – 6 independent animals each condition (comprising 125 mitochondria from 38 cells, control; \geq 250 mitochondria, from \geq 60 cells per group after TGI; ** indicates $p < 0.01$ by one way ANOVA with Tukey post hoc).

Ischemia-induced mitochondrial Zn^{2+} accumulation correlates with ultrastructural disruption

We next set out to use the Timm's sulfide silver labeling technique to localize sites of neuronal Zn^{2+} accumulation at an ultrastructural level. As indicated above, this technique inserts metallic silver deposits at sites of labile or loosely bound Zn^{2+} accumulation. Staining in neurons is considered to be quite specific for Zn^{2+} , and was found to be entirely absent in mice lacking the vesicular Zn^{2+} transporter (ZnT3 knockout mice) [14]. In control studies seeking to further validate the Zn^{2+} specificity of the stain, we made use of the well characterized hippocampal slice oxygen glucose deprivation (OGD) model of brain ischemia [20-22]. As in Fig. 1B, in control slices Timm staining was present in the mossy fiber pathway but was completely absent in the pyramidal cell layer, but distinct label appeared in the pyramidal cell layer after a brief (8 min) episode of OGD. However, when the slices were perfused with the Zn^{2+} preferring chelator, N,N,N',N'-tetrakis(2-pyridylmethyl)ethylenediamine (TPEN) after OGD, the Timm's label was markedly diminished (data not shown), providing further support to the contention that the Timm's stain largely reflects accumulation of labile Zn^{2+} in post-synaptic neurons, as has been previously described.

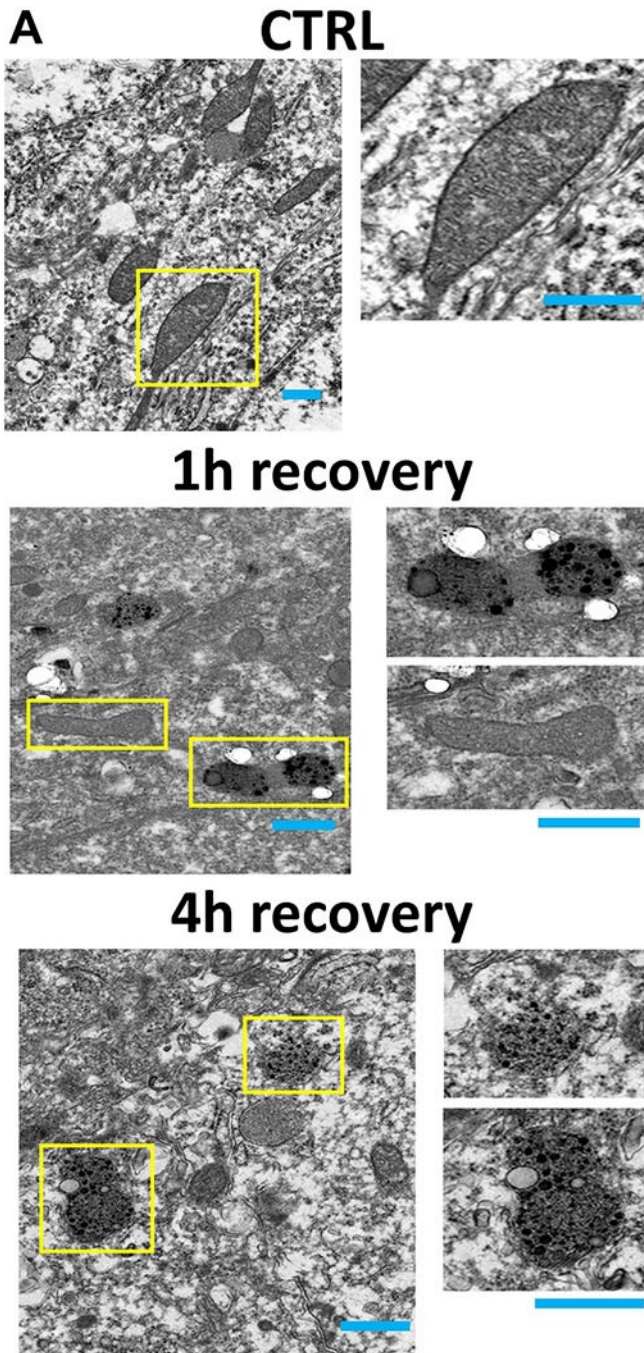
Timm's labeled slices were subjected to TEM examination in order to investigate the redistribution of labile Zn^{2+} in the somata of CA1 pyramidal neurons in rats subjected to TGI as above. This approach is particularly well suited for the ultrastructural examination of Zn^{2+} localization, as the silver deposit is electron dense and thus easily visualized. Timm's labeling

and TEM examination are strongly dependent upon animal perfusion and tissue processing techniques. Prior studies have employed a number of variations to try to optimize both the visualization of the Zn^{2+} and the preservation of the tissue ultrastructure for TEM examination. A key component of Timm's labeling is the early use of Na_2S in the perfusion procedure to precipitate the labile Zn^{2+} *in situ*. In early trials we carried out two distinct variations (see **Materials and Methods** for full details): **1.** Initial perfusion with Na_2S (0.2% in buffer, 5 min) prior to perfusion with PFA/glutaraldehyde, in order to maximize Zn^{2+} detection by fixing it *in situ* at the earliest possible time point; or **2.** Perfusion with PFA/glutaraldehyde (5 min) prior to Na_2S (0.4%, 7 min), in order to optimize tissue preservation. In both cases perfusion was followed by brain removal and post-fixation incorporating PFA, glutaraldehyde, and Na_2S . In control slices subjected to these two perfusion protocols we noted no qualitative difference in the appearance or localization of the Timm's label, and opted for the second approach (fixation first), which is the more conservative in terms of Zn^{2+} detection, in subsequent experiments.

In our ultrastructural studies, hippocampal CA1 sections from 10 animals (3 controls, 4 ischemia followed by 1 h recovery; 3 ischemia followed by 4 h recovery) were subjected to blinded quantitative examination. In agreement with prior studies [8, 14], in control rats, we found electron dense Zn^{2+} foci to be most evident in presynaptic mossy fiber boutons with little evidence of Zn^{2+} at other loci or within neuronal somata. In the controls, a substantial majority of mitochondria appeared healthy and intact; these generally were elongated, and had distinct cristae structure visible along with an intact double outer membrane (**Figs. 3A, 4A**). However, a minority (~20-25%) showed evidence of mild injury; these were generally more round than elongated suggestive of early swelling, and often showed some disruption or blurring of their cristae. Interestingly, close to 50% of these mildly damaged mitochondria contained apparent Zn^{2+} deposits, as indicated by the presence of electron dense silver granules similar to those seen in presynaptic boutons. In contrast, Zn^{2+} deposits were only seen in a very small fraction (<1%) of intact appearing mitochondria, in all conditions.

In comparison to the controls, the numbers of damaged mitochondria were substantially increased after global ischemia. With 1 h recovery, ~50% of mitochondria were damaged.

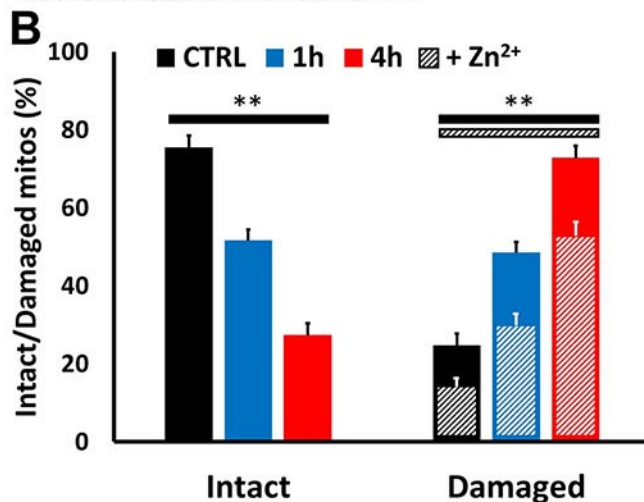
Interestingly the damage appeared to be strongly progressive, with >75% of mitochondria



showing damage after 4 h recovery. Furthermore, at each of these recovery time points, the majority of damaged mitochondria had clear Zn^{2+} deposits (**Fig. 3B**) supporting a Zn^{2+} contribution to the mitochondrial damage. Yet, in each condition, a minority of damaged mitochondria lacked clear Zn^{2+} deposits. The reasons for this are not completely clear but may well reflect a number of factors, including: **1.** A threshold level of Zn^{2+} accumulation may be needed for detection by the Timm's labeling procedure; **2.** The use of our conservative perfusion paradigm, which maximizes structural protection / integrity at the possible expense of some loss of Zn^{2+} from loci of intracellular accumulation, and **3.** Contributions of Zn^{2+} independent mitochondrial swelling mechanisms.

Figure 3. Global ischemia induces progressive Zn^{2+} accumulation and injury in CA1 pyramidal neuronal mitochondria. Rats were subjected to TGI followed by 1 or 4h recovery. To assess mitochondrial damage and Zn^{2+} accumulation in CA1 pyramidal neurons, Timm's labeled hippocampal slices were examined under TEM.

A. Representative electron micrographs. Representative TEM images (4000x) of Timm's labeled slices from a control rat (top), or rats subjected to ischemia followed by 1 h (middle), or 4 h (bottom) recovery (Bar = 0.5 μm ; rectangles show regions displayed at greater magnification, right; Bar = 0.5 μm) Note the intact structure and absence of Timm's precipitate in most mitochondria in control, the significant numbers of mitochondria showing early damage (with rounding) and distinct presence of Timm's precipitate with 1 h recovery, with greater numbers of mitochondria displaying Zn^{2+} accumulation and extensive injury after 4 h recovery.

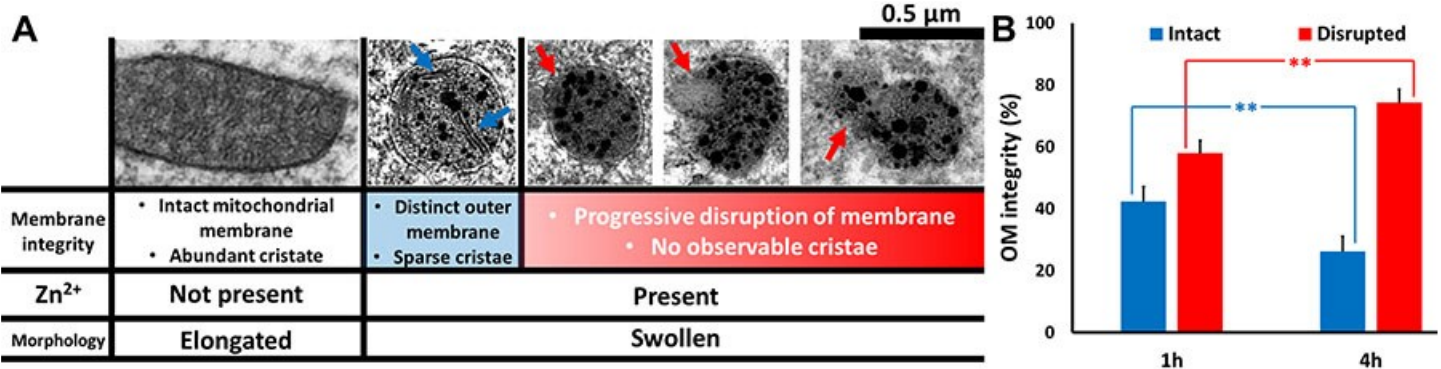


B. Quantitative evaluation. To assess

mitochondrial Zn^{2+} accumulation and damage, all evident mitochondria in images from CA1 pyramidal neurons were rated by an observer blinded to the experimental condition. Bars display percentage of mitochondria appearing intact or showing evidence of damage (assessed as described), and hatchmarks indicate the presence of evident Zn^{2+} deposits in the damaged mitochondria (Zn^{2+} deposits were only present in $< 1\%$ of intact appearing mitochondria, in all conditions). Note the marked increase in numbers of damaged appearing mitochondria after ischemia, the marked increase in their numbers with increased recovery duration (from 1 to 4 h), and the parallel increase in numbers containing distinct Zn^{2+} deposits, present in the majority of damaged mitochondria in each condition. Values represent mean \pm SEM from 3 - 4 independent animals each condition (for each animal, ≥ 70 mitochondria from ≥ 10 sections were rated; ** indicates $p < 0.01$ by one way ANOVA with Tukey post hoc).

We further sought to discriminate degrees of mitochondrial damage related to mitochondrial Zn^{2+} accumulation (**see Fig. 4**). As noted above, all the damaged mitochondria showed evidence of mild swelling and early disruption of cristae structure. However, some showed more extreme disruption or even complete absence of evident cristae. In some there was apparent vacuole formation within mitochondria, whereas others showed varying degrees of outer membrane (**OM**) rupture, progressing from a small area of rupture to complete loss of evident outer membrane. In some mitochondria with apparent severe outer membrane rupture, there was apparent “leakage” of Zn^{2+} containing material into the surrounding cytoplasm (see images, **Fig 4A**). These characteristics are suggestive of progressive stages of mitochondrial damage.

To further address the possible progression of the mitochondrial damage and disruption, we carried out a second blinded count and rating of mitochondria from the same set of post-ischemic images, but only evaluating the mitochondria that both appeared damaged and contained Zn^{2+} precipitates. In this assessment we separated the mitochondria on the basis of the integrity of their OMs, considering that a ruptured OM reflected relatively severe and likely irrecoverable damage. Interestingly, we found the distribution of the mitochondrial damage to differ substantially between 1 and 4 h recovery, with the proportion of mitochondria with



ruptured OM's being far greater with 4 h recovery (**Fig. 4B**).

Figure 4. Discrimination of degrees of mitochondrial damage: progression of mitochondrial disruption with time of recovery.

A. Graded degrees of mitochondrial structural disruption: Discriminating criteria and representative images. Table illustrates the spectrum of mitochondrial morphologies as described. To be rated as intact, mitochondria were generally elongated and had intact outer membrane and clear abundant cristae. Mitochondria were rated as showing mild damage if they showed evidence of early swelling and some loss of cristae but with an intact outer membrane (**blue arrows** highlight sparse cristae), and were considered to be severely damaged if there was apparent disruption of the outer membrane (**red arrows**); virtually all mitochondria with outer membrane rupture showed no discernable cristae. Such severely damaged mitochondria also displayed a spectrum of damage, ranging from early membrane rupture (left) to substantial rupture with loss of mitochondria contents (middle) or complete absence of membrane (right).

B. Mitochondrial damage progresses with increasing recovery time. To assess possible progression of mitochondrial disruption over time after ischemia, we re-examined the same post-ischemic images (as in Fig. 3), only evaluating the mitochondria that both appeared damaged and contained Zn^{2+} precipitates. Each mitochondrion was rated as mildly damaged if it was judged to have an intact outer membrane (**OM**; **blue**) or severely damaged if its OM was disrupted (**red**). Note the substantial progression of mitochondrial disruption over time, with a far greater percentage of mitochondria showing OM disruption after 4 h than after 1 h recovery. Bars show percentage of injured mitochondria in each category (intact or disrupted OM), and represent mean \pm SEM from 3 - 4 independent animals (≥ 55 mitochondria counted from ≥ 10 sections, each animal; ** indicates $p < 0.01$ by 2-tailed student's t test).

Thus, present observations reveal that both the presence of Zn^{2+} accumulation within mitochondria and the extent of damage of the Zn^{2+} containing mitochondria are progressive in the hours after an episode of transient global ischemia. Whereas this does not prove that the Zn^{2+} causes the mitochondrial damage, the data are certainly consistent with a model **we have proposed based upon recent hippocampal slice studies [19, 22]** wherein progressive Zn^{2+} accumulates in mitochondria both during and for a considerable period of time after the ischemic episode, contributing to their progressive damage and disruption.

Discussion

Summary of findings

Despite strong evidence for Zn^{2+} contributions to neuronal injury in ischemia and after prolonged seizures, with accumulation of labile Zn^{2+} in many degenerating neurons and neuroprotective effects of Zn^{2+} chelation, as well as numerous clues that mitochondria are likely to be important sites of injurious Zn^{2+} effects, the relationship between mitochondrial Zn^{2+} accumulation, mitochondrial disruption and neuronal injury *in vivo* has not been previously examined. The

present study is the first to use the Timm's labeling approach – which yields electron dense silver deposits at sites of labile Zn^{2+} accumulation – in order to examine the redistribution of Zn^{2+} in CA1 pyramidal neurons after *in vivo* TGI at the ultrastructural level. Notably, in these post-ischemic neurons, we found a strong relationship between the appearance of Timm's deposit within mitochondria with their swelling and structural disruption. This observation provides new support to the idea that the Zn^{2+} contributes to the mitochondrial damage / dysfunction seen in these neurons. Furthermore, examination at 2 time points after TGI revealed a progression in both numbers of damaged and Zn^{2+} containing mitochondria as well as in the degree of their disruption. This delayed temporal evolution correlates with the delayed injury associated with mitochondrial disruption that is characteristic of CA1 pyramidal neurons after ischemia [23-25], and suggests the possibility that the mitochondrial Zn^{2+} accumulation and its consequences may be progressive events during the hours post-ischemia that are amenable to delayed therapeutic interventions.

Zn^{2+} in ischemic hippocampal injury

As noted above, a small portion of brain Zn^{2+} is loosely bound and can be detected histochemically using Timm's labeling or visualized with membrane permeable fluorescent markers; under normal conditions, this pool largely comprises Zn^{2+} present in presynaptic vesicles of some excitatory pathways (most prominently in large mossy fiber boutons) [8, 12]. Thus, observations that labile Zn^{2+} accumulates in injured and degenerating neurons after prolonged seizures or ischemia and that these effects were attenuated by an extracellular Zn^{2+} chelator led to the presumption that they resulted from presynaptic Zn^{2+} release and its “translocation” into the postsynaptic neurons [3-5]. This idea was tested via use of mice lacking the ZnT3 vesicular Zn^{2+} transporter, which are entirely lacking in presynaptic vesicular Zn^{2+} [14]. Surprisingly, seizure induced Zn^{2+} accumulation and injury to CA1 pyramidal neurons was actually increased in ZnT3 knockout mice, indicating a distinct non-synaptic source of toxic Zn^{2+} accumulation in these neurons [31].

A likely candidate source was Zn^{2+} that is bound to Zn^{2+} -buffering proteins like MT-III (the primary metallothionein isoform in neurons) [32]. Indeed, studies in neuronal culture revealed that strong Zn^{2+} mobilization from these proteins could trigger Zn^{2+} -dependent neuronal injury in the absence of extracellular Zn^{2+} entry [33, 34]. The generation of MT-III knockouts provided a model to directly examine the contributions of Zn^{2+} release from this protein [35]. *In vivo* seizure studies, as well as hippocampal slice OGD studies, using both ZnT3 and MT-III KO's highlighted distinct contributions of these pools of Zn^{2+} to the Zn^{2+} accumulation and injury that occurred, with mobilization from MT-III predominating in CA1, but with presynaptic release and translocation into postsynaptic neurons appearing to predominate in CA3 [15, 20, 22], which receives strong synaptic input from the Zn^{2+} rich mossy fiber terminals, and in contrast to CA1 neurons are preferentially injured after prolonged limbic seizures.

Mitochondria are likely to be important targets of Zn^{2+} effects

Despite the considerable evidence that “excitotoxic” mechanisms are important contributors to neurodegeneration occurring after acute brain insults including ischemia, trauma and prolonged seizures, many downstream mechanisms have been implicated and there are as yet no neuroprotective treatments that have shown clear benefit in humans. As discussed, early studies focused on the key role of Ca^{2+} entry through highly Ca^{2+} permeable NMDA channels. Studies of relevant downstream mechanisms highlighted mitochondria as a likely important site of Ca^{2+} effects, with Ca^{2+} entering mitochondria through the mitochondrial Ca^{2+} uniporter (**MCU**), and with sufficiently large mitochondrial loads, triggering deleterious effects including reactive oxygen species generation and opening of the permeability transition pore, leading to release of apoptotic mediators including cytochrome C [36]. However, it has also become apparent that Zn^{2+} has very potent effects on mitochondria. This slow recognition of likely Zn^{2+} contributions reflects in part the relatively recent availability of Zn^{2+} selective indicators [37]. Indeed, virtually all the available “ Ca^{2+} indicators” respond to Zn^{2+} with greater potency, a factor that likely led to the mistaken attribution of some Zn^{2+} effects to Ca^{2+} [38, 39].

In many studies on isolated mitochondria and cultured neurons, application of Zn^{2+} appeared to disrupt mitochondrial function with a high degree of potency [40-44]. However, some studies have found Zn^{2+} to induce effects on mitochondria with more modest potency, and clues have emerged to factors underlying these divergent results [for review see [19]]. One key variable concerns the levels of free Zn^{2+} achieved in intact neurons upon exogenous exposure. This depends both upon the route of Zn^{2+} entry [44] but also critically upon the integrity of Zn^{2+} buffering by MTs and related peptides [18, 43, 45]. Another likely variable concerns Zn^{2+} interactions with Ca^{2+} , with synergism between effects of these ions on mitochondria [18, 42, 46], and possible dependence upon Ca^{2+} for Zn^{2+} to enter mitochondria through the MCU [47-50].

Whereas above studies of Zn^{2+} effects on mitochondria applied Zn^{2+} to isolated mitochondria or cultured neurons, there is also evidence that endogenous Zn^{2+} accumulates in mitochondria, contributing to their dysfunction after *in vivo* ischemia [6, 17]. In addition, studies in our acute hippocampal slice OGD ischemia model provide evidence that early Zn^{2+} uptake into mitochondria via the MCU occurs upstream from and contributes to the subsequent sharp terminal Ca^{2+} rise [20, 21]. More recently, we have subjected slices to sublethal OGD, terminating the exposure shortly after the initial Zn^{2+} rise but before the terminal Ca^{2+} rise, in order to model events that may occur after transient *in vivo* ischemia. Interestingly, consistent with present observations after *in vivo* TGI, we found evidence for delayed and progressive Zn^{2+} uptake into mitochondria of CA1 pyramidal neurons after OGD termination which appeared to contribute to delayed mitochondrial swelling. In contrast, in CA3 neurons mitochondrial Zn^{2+} recovered rapidly after OGD termination [22].

Conclusions and Future Directions

The development of neuroprotective interventions for stroke has presented an extremely difficult challenge, for both logistical reasons and incomplete understanding of critical events in the injury cascade. Studies over the past two decades have made it progressively clear that Zn^{2+} is an important ionic mediator of the excitotoxic injury cascade in CA1 as well as in many

forebrain neurons in which it accumulates. Paralleling the evolving evidence for Zn^{2+} contributions in ischemia, there has been a rapid increase in understanding of ways in which Zn^{2+} injures neurons, and in particular, emerging clues that mitochondria might be important targets of its early effects, with compelling clues from both *in vivo* and slice models highlighting large and long lasting effects after transient ischemia in CA1 [19].

Yet, until now, no study has specifically examined the relationship between mitochondrial Zn^{2+} accumulation, mitochondrial disruption and neuronal injury after *in vivo* ischemia. Such a study requires an ultrastructural approach, to correlate Zn^{2+} accumulation with organelle morphology at the individual mitochondrion level, and the presently employed Timm's labeling (to fix Zn^{2+} *in situ*) combined with TEM would seem ideally suited for such an investigation. Present findings in a rat TGI model demonstrate, for the first time, progressive Zn^{2+} accumulation in CA1 mitochondria to be strongly correlated with their physical disruption. While this does not in itself indicate causation, it provide new support for a possible direct contributory role of the mitochondrial Zn^{2+} in the delayed mitochondria damage and cell death that are characteristic of CA1 [23-25].

Future aims will seek to assess potential therapeutic utility of targeting these early events. Relevant questions include the nature of interventions that may provide benefit, the temporal window of opportunity to intervene, and the definition of contributions of Zn^{2+} / mitochondrial interactions in neuronal populations other than CA1 in which early Zn^{2+} accumulation occurs. We hope these insights will aid the development of therapeutic interventions that improve outcomes when delivered after ischemia.

Acknowledgements: Supported by NIH grants NS096987 and NS100494 (JHW), and the American Heart Association grants 17GRNT33410181 (JHW) and 16PRE29560003 (SGJ). The authors declare no competing financial interests. We wish to thank Oswald Steward and Ilse Sears-Kraxberger for excellent support and help with the electron microscopy.

References

1. Hoyte L, Barber PA, Buchan AM, et al., The rise and fall of NMDA antagonists for ischemic stroke. *Curr Mol Med* 2004; 4(2):131-6
2. Ikonomidou C and Turski L, Why did NMDA receptor antagonists fail clinical trials for stroke and traumatic brain injury? *Lancet Neurol* 2002; 1(6):383-6
3. Frederickson CJ, Hernandez MD, and McGinty JF, Translocation of zinc may contribute to seizure-induced death of neurons. *Brain Res* 1989; 480(1-2):317-21
4. Koh JY, Suh SW, Gwag BJ, et al., The role of zinc in selective neuronal death after transient global cerebral ischemia. *Science* 1996; 272(5264):1013-6
5. Tonder N, Johansen FF, Frederickson CJ, et al., Possible role of zinc in the selective degeneration of dentate hilar neurons after cerebral ischemia in the adult rat. *Neurosci Lett* 1990; 109(3):247-52
6. Calderone A, Jover T, Mashiko T, et al., Late calcium EDTA rescues hippocampal CA1 neurons from global ischemia-induced death. *J Neurosci* 2004; 24(44):9903-13
7. Yin HZ, Sensi SL, Ogoshi F, et al., Blockade of Ca^{2+} -permeable AMPA/kainate channels decreases oxygen-glucose deprivation-induced Zn^{2+} accumulation and neuronal loss in hippocampal pyramidal neurons. *J Neurosci* 2002; 22(4):1273-9
8. Perez-Clausell J and Danscher G, Intravesicular localization of zinc in rat telencephalic boutons. A histochemical study. *Brain Res* 1985; 337(1):91-8
9. Assaf SY and Chung SH, Release of endogenous Zn^{2+} from brain tissue during activity. *Nature* 1984; 308(5961):734-6
10. Howell GA, Welch MG, and Frederickson CJ, Stimulation-induced uptake and release of zinc in hippocampal slices. *Nature* 1984; 308(5961):736-8
11. Sloviter RS, A selective loss of hippocampal mossy fiber Timm stain accompanies granule cell seizure activity induced by perforant path stimulation. *Brain Res* 1985; 330(1):150-3
12. Frederickson CJ, Rampy BA, Reamy-Rampy S, et al., Distribution of histochemically reactive zinc in the forebrain of the rat. *J Chem Neuroanat* 1992; 5(6):521-30
13. Haug FM, Electron microscopical localization of the zinc in hippocampal mossy fibre synapses by a modified sulfide silver procedure. *Histochemie* 1967; 8(4):355-68
14. Cole TB, Wenzel HJ, Kafer KE, et al., Elimination of zinc from synaptic vesicles in the intact mouse brain by disruption of the ZnT3 gene. *Proc Natl Acad Sci U S A* 1999; 96(4):1716-21
15. Lee JY, Kim JH, Palmiter RD, et al., Zinc released from metallothionein-iii may contribute to hippocampal CA1 and thalamic neuronal death following acute brain injury. *Exp Neurol* 2003; 184(1):337-47
16. Shuttleworth CW and Weiss JH, Zinc: new clues to diverse roles in brain ischemia. *Trends Pharmacol Sci* 2011; 32(8):480-6
17. Bonanni L, Chachar M, Jover-Mengual T, et al., Zinc-dependent multi-conductance channel activity in mitochondria isolated from ischemic brain. *J Neurosci* 2006; 26(25):6851-62
18. Ji SG and Weiss JH, Zn^{2+} -induced disruption of neuronal mitochondrial function: Synergism with Ca^{2+} , critical dependence upon cytosolic Zn^{2+} buffering, and contributions to neuronal injury. *Exp Neurol* 2018; 302:181-195
19. Ji SG, Medvedeva YV, Wang HL, et al., Mitochondrial Zn^{2+} Accumulation: A Potential Trigger of Hippocampal Ischemic Injury. *Neuroscientist* 2018:1073858418772548
20. Medvedeva YV, Lin B, Shuttleworth CW, et al., Intracellular Zn^{2+} accumulation contributes to synaptic failure, mitochondrial depolarization, and cell death in an acute slice oxygen-glucose deprivation model of ischemia. *J Neurosci* 2009;

29(4):1105-14

21. Medvedeva YV and Weiss JH, Intramitochondrial Zn(2+) accumulation via the Ca(2+) uniporter contributes to acute ischemic neurodegeneration. *Neurobiol Dis* 2014; 68:137-44
22. Medvedeva YV, Ji SG, Yin HZ, et al., Differential Vulnerability of CA1 versus CA3 Pyramidal Neurons After Ischemia: Possible Relationship to Sources of Zn²⁺ Accumulation and Its Entry into and Prolonged Effects on Mitochondria. *J Neurosci* 2017; 37(3):726-737
23. Colbourne F, Sutherland GR, and Auer RN, Electron microscopic evidence against apoptosis as the mechanism of neuronal death in global ischemia. *J Neurosci* 1999; 19(11):4200-10
24. Kirino T, Delayed neuronal death in the gerbil hippocampus following ischemia. *Brain Res* 1982; 239(1):57-69
25. Sugawara T, Fujimura M, Morita-Fujimura Y, et al., Mitochondrial release of cytochrome c corresponds to the selective vulnerability of hippocampal CA1 neurons in rats after transient global cerebral ischemia. *J Neurosci* 1999; 19(22):RC39
26. Kang YJ, Tian G, Bazrafkan A, et al., Recovery from Coma Post-Cardiac Arrest Is Dependent on the Orexin Pathway. *J Neurotrauma* 2017; 34(19):2823-2832
27. Crouzet C, Wilson RH, Bazrafkan A, et al., Cerebral blood flow is decoupled from blood pressure and linked to EEG bursting after resuscitation from cardiac arrest. *Biomed Opt Express* 2016; 7(11):4660-4673
28. Victorov IV, Prass K, and Dirnagl U, Improved selective, simple, and contrast staining of acidophilic neurons with vanadium acid fuchsin. *Brain Res Brain Res Protoc* 2000; 5(2):135-9
29. Danscher G and Zimmer J, An improved Timm sulphide silver method for light and electron microscopic localization of heavy metals in biological tissues. *Histochemistry* 1978; 55(1):27-40
30. Park J, Trinh VN, Sears-Kraxberger I, et al., Synaptic ultrastructure changes in trigeminocervical complex posttrigeminal nerve injury. *J Comp Neurol* 2016; 524(2):309-22
31. Lee JY, Cole TB, Palmiter RD, et al., Accumulation of zinc in degenerating hippocampal neurons of ZnT3-null mice after seizures: evidence against synaptic vesicle origin. *J Neurosci* 2000; 20(11):RC79
32. Maret W, Metallothionein/disulfide interactions, oxidative stress, and the mobilization of cellular zinc. *Neurochem Int* 1995; 27(1):111-7
33. Aizenman E, Stout AK, Hartnett KA, et al., Induction of neuronal apoptosis by thiol oxidation: putative role of intracellular zinc release. *J Neurochem* 2000; 75(5):1878-88
34. Bossy-Wetzel E, Talantova MV, Lee WD, et al., Crosstalk between Nitric Oxide and Zinc Pathways to Neuronal Cell Death Involving Mitochondrial Dysfunction and p38-Activated K(+) Channels. *Neuron* 2004; 41(3):351-65
35. Erickson JC, Hollopeter G, Thomas SA, et al., Disruption of the metallothionein-III gene in mice: analysis of brain zinc, behavior, and neuron vulnerability to metals, aging, and seizures. *J Neurosci* 1997; 17(4):1271-81
36. Nicholls DG and Budd SL, Mitochondria and neuronal survival. *Physiol Rev* 2000; 80(1):315-60
37. Gee KR, Zhou ZL, Ton-That D, et al., Measuring zinc in living cells. A new generation of sensitive and selective fluorescent probes. *Cell Calcium* 2002; 31(5):245-51
38. Cheng C and Reynolds IJ, Calcium-sensitive fluorescent dyes can report increases in intracellular free zinc concentration in cultured forebrain neurons. *J Neurochem*

1998; 71(6):2401-10

39. Stork CJ and Li YV, Intracellular zinc elevation measured with a "calcium-specific" indicator during ischemia and reperfusion in rat hippocampus: a question on calcium overload. *J Neurosci* 2006; 26(41):10430-7
40. Dineley KE, Richards LL, Votyakova TV, et al., Zinc causes loss of membrane potential and elevates reactive oxygen species in rat brain mitochondria. *Mitochondrion* 2005; 5(1):55-65
41. Gazaryan IG, Krasinskaya IP, Kristal BS, et al., Zinc irreversibly damages major enzymes of energy production and antioxidant defense prior to mitochondrial permeability transition. *J Biol Chem* 2007; 282(33):24373-80
42. Jiang D, Sullivan PG, Sensi SL, et al., Zn(2+) induces permeability transition pore opening and release of pro-apoptotic peptides from neuronal mitochondria. *J Biol Chem* 2001; 276(50):47524-9
43. Sensi SL, Ton-That D, Sullivan PG, et al., Modulation of mitochondrial function by endogenous Zn²⁺ pools. *Proc Natl Acad Sci U S A* 2003; 100(10):6157-62
44. Sensi SL, Yin HZ, Carriedo SG, et al., Preferential Zn²⁺ influx through Ca²⁺-permeable AMPA/kainate channels triggers prolonged mitochondrial superoxide production. *Proc Natl Acad Sci U S A* 1999; 96(5):2414-9
45. Clausen A, McClanahan T, Ji SG, et al., Mechanisms of Rapid Reactive Oxygen Species Generation in response to Cytosolic Ca²⁺ or Zn²⁺ Loads in Cortical Neurons. *Plos One* 2013; 8(12):e83347
46. Sensi SL, Yin HZ, and Weiss JH, AMPA/kainate receptor-triggered Zn²⁺ entry into cortical neurons induces mitochondrial Zn²⁺ uptake and persistent mitochondrial dysfunction. *Eur J Neurosci* 2000; 12(10):3813-8
47. Saris NE and Niva K, Is Zn²⁺ transported by the mitochondrial calcium uniporter? *FEBS Lett* 1994; 356(2-3):195-8
48. De Stefani D, Patron M, and Rizzuto R, Structure and function of the mitochondrial calcium uniporter complex. *Biochim Biophys Acta* 2015; 1853(9):2006-11
49. Kamer KJ and Mootha VK, The molecular era of the mitochondrial calcium uniporter. *Nat Rev Mol Cell Biol* 2015; 16(9):545-53
50. Marchi S and Pinton P, The mitochondrial calcium uniporter complex: molecular components, structure and physiopathological implications. *J Physiol* 2014; 592(Pt 5):829-39